in a high Nb fully lamellar TiAl Alloy. *Scripta Materialia*. 2003. Vol. 48. pp. 79–84

21. Jin Y., Wang J. N., Yang J., Wang Y. Microstructure refinement of cast TiAl alloys by solidification. *Scripta Materialia*. 2004. No. 51. pp. 113–117.

22. Hao Y. L., Yang R., Cui Y. Y., Li D. The influence of alloying on the $\alpha_2/(\alpha_2 + \gamma)$ phase boundaries in TiAl based systems. *Acta Materialia*. 2000. Vol. 48. pp. 1313–1324.

23. Kainuma R., Fujita Y., Mitsui H., Ishida K. Phase equilibria among α (hcp), β (bcc) and γ ($L1_0$) phases in Ti – Al base ternary alloys. *Intermetallics*. 2000. No. 8. pp. 855–867.

24. Witusiewicz V. T., Bondar A. A., Hecht U., Velikanova T. Ya. The Al–B–Nb–Ti system: IV. Experimental study and thermodynamic reevaluation of the binary Al–Nb and ternary Al – Nb – Ti systems. *Journal of Alloys and Compounds*. 2009. No. 472. pp. 133–161.

25. Andersson J. O., Helander T., Hoglund L., Shi P. F., Sundman B. Thermo-Calc and DICTRA, computational tools for materials science, *Calphad*. 2002. Vol. 26. pp. 273–312.

26. Werner R., Schloffer M., Schwaighofer E., Clemens H., Mayer S. Thermodynamic calculations of phase equilibria and phase fractions of a β-solidifying TiAl alloy using the CALPHAD approach. *MRS Proceedings*. 2013. pp. 15–16.

27. Clemens H., Mayer S. Design, processing, microstructure, properties, and applications of advanced intermetallic TiAl alloys. *Advanced Engineering Materials*. 2013. No. 15. pp. 191–215.

28. Belov N. A., Akopyan T. K., Belov V. D., Gorshenkov M. V., Gershman J. S. The effect of Cr and Zr on the structure and phase composition of TNM gamma titanium aluminide alloy. *Intermetallics*. 2017. Vol. 84. pp. 121–129.

Microstructure and phase composition of the eutectic Al – Ca alloy, additionally alloyed with small additives of zirconium, scandium and manganese

N. A. Belov, Professor of the Department of Metal Forming[1], e-mail: nikolay-belov@yandex.ru
K. A. Batyshev, Professor[2]
V. V. Doroshenko, Post-Graduate Student of the Department of Metal Forming[1]

[1] National University of Science and Technology MISiS, Moscow, Russia.
[2] Bauman Moscow State Technical University, Moscow, Russia.

Using both thermodynamic calculations and experimental analyses, the Al – Ca – Mn – Fe – Zr – Sc phase diagram near the aluminum corner has been studied. Based on the obtained results, the optimal concentrations of calcium (about 4%) and manganese (about 0.7%) at an allowable iron content of up to 0.3–0.4% were chosen. According to the thermodynamic calculations, during solidification of the Al4Ca0.7Mn0.4Fe alloy, after formation of a the (Al) primary crystals, the eutectic reaction $L \to$ (Al) + + Al_6(Fe, Mn) should occur. Solidification of this alloy should be completed via the ternary eutectic reaction $L \to$ (Al) + Al_6(Fe, Mn) + Al_4Ca. The addition of 0.2–0.4% zirconium should leads to the formation of primary crystals of the Al_3Zr aluminide. However, it is known that at the cooling rates typical for the casting in metal moulds (5–20 ºC/s), the concentration boundary is shifted toward higher zirconium concentrations. Therefore, it was assumed that the total amount of Zr should enter into the (Al) composition and consequently have no influence on the phase composition of the alloy. When zirconium addition is present, the casting temperature should be higher than for the base alloy. The microstructure of two alloys with different content of zirconium and scandium: Al4Ca0.7Mn0.4Fe0.2Zr0.1Sc and Al4Ca0.7Mn0.4Fe0.4Zr was examined by means of optical microscopy, scanning electron microscopy and by electron microprobe analysis. The obtained results have revealed that for both alloys microstructure consists of the (Al) primary crystals and eutectic colonies with a fine structure. Calcium and iron are concentrated in the eutectic, while scandium, zirconium and manganese were detected in the both eutectic composition and (Al) primary crystals. Analysis of the hardness and specific electrical conductivity together with transmission electron microscopy has revealed that joint alloying with zirconium and scandium (0.20% Zr and 0.1% Sc) leads to the precipitation hardening due to the decomposition of (Al) and further precipitation of the coherent $L1_2 – Al_3$(Zr, Sc) phase nanoparticles. The highest hardness is observed after step annealing at 250 ºC, 3 h plus 300 ºC, 3 h.

Key words: Al – Ca alloys, Al_3(Zr, Sc) nanoparticles, thermodynamic calculations, phase transformations, microstructure, annealing, hardening.

DOI: 10.17580/nfm.2017.02.09

Introduction

The Al − Ca system is promising for the development of a new generation of cast and wrought aluminum alloys [1−4]. Calcium, as well as silicon, forms a eutectic-type diagram with aluminium (in the aluminum rich region). However, unlike silicon, calcium forms intermetallic Al4Ca phase, the fraction of which in the binary (Al) + + Al$_4$Ca eutectic exceeds 30% (vol.), what is three times that in the (Al) + (Si) eutectic. Among other advantages, calcium with respect to the content in the Earth's core (3.6% (wt.)) occupies the third place among the metals (yielding only to aluminum and iron) and its density is 1.542 g/cm^3, which can be used to reduce the weight of aluminum alloys. This allows us to achieve a unique set of properties additively depending on the fraction of structural components. For instance, in [4], it was shown that the Al − Ca − Mg − Si system (in particular, the region near the Al10Mg3Ca1Si alloy) is quite suitable as a basis for the development of light corrosion resistant alloys with a "eutectic composite" type structure.

At present, one of the trends in the development of aluminum alloys is the use of small additions of scandium and zirconium to achieve hardening of alloys without quenching operation [5, 6]. Scandium is one of the most effective hardeners in aluminium alloys, due to the formation of Al$_3$Sc (L1$_2$) phase coherent nanoparticles during the simple annealing at temperatures near 300 ^{o}C [7, 8]. However, scandium is a very expensive metal, so its use as an additive in industrial production is severely limited. The most effective method is the introduction of scandium together with cheaper zirconium [9−13].

Despite the significant advantages by alloying with zirconium and scandium, it should be noted that they are not compatible with any systems. In Al − Si alloys, which are the main group (3xx series) of casting aluminium alloys, the introduction of scandium and zirconium is useless, since it does not lead to appreciable hardening [1]. In contrast, for the alloys of the eutectic Al − Ni system, the additions of zirconium and scandium make it possible to achieve substantial hardening. However, nickel leads to a decrease in the corrosion resistance, as well as an increase in alloy density. Therefore, it is advisable to consider other alloying systems, in particular, those based on the aluminium-calcium eutectic [2, 14]. In the work [1], the principal possibility of creating such Al − Ca based eutectic alloys was justified. For the further development of this class alloys, it is necessary to consider the possibility of creating sparingly alloyed Al − Ca alloys, containing besides scandium also zirconium and manganese to achieve maximum hardening. We should also take into account the influence of the inevitable iron impurity on the phase composition of the new alloys.

Based on the above, the main purpose of this work is to analyze the phase composition, microstructure and precipitation hardening effect due to formation of the L1$_2$ − Al$_3$(Zr, Sc) phase nanoparticles of the model hypoeutectic alloys based on the Al − Ca − Fe − Mn system. It is convenient to analyse the phase composition of the alloys of such multicomponent systems using thermodynamic calculations. For this purpose, we used the Thermo-Calc program and a commercially available thermodynamic database TTAL5.

Experimental methods

The main subject of the experimental study is the alloy of the selected composition (hereinafter Al4CaMnFeZrSc). The melting was carried out in an electric resistance furnace in a graphite-chased crucible based on high purity aluminium (99.99%). Calcium, manganese, iron, zirconium and scandium were introduced into the aluminium melt in the form of binary master alloys (Al − 15% Ca, Al − 10% Mn, Al − 10% Fe, Al − 15% Zr and Al − 2% Sc, respectively). The casting was carried out in a graphite mould to obtain flat ingots with dimensions of 15×30×180 mm (the cooling rate during solidification was ~10 K/s). Samples were extracted from the obtained castings to study the structure and properties. The chemical composition of the experimental alloys is given in Table 1.

The heat treatment of the castings was carried out in muffle electric furnaces with a temperature accuracy of ~3 K. Multi-step annealing modes in the temperature range from 250 to 500 ^{o}C with a step of 50 ^{o}C and a 3-h exposure at each step (Table 2) were used. After each annealing step, the samples were cooled in air. The stepwise mode allows us to carry out all studies of the influence of heating temperatures on one sample. This method was both informative and economical for the Al alloys, which hardened due to the nanoparticles of the L1$_2$ phase [1, 15].

The microstructure was examined by means of optical microscopy (OM, Olympus GX51), transmission electron

Table 1

Chemical composition of experimental alloys

№	Alloy	Chemical composition, % (wt.)					
		Al	Ca	Mn	Fe	Zr	Sc
1	Al4Ca0.7Mn0.4Fe0.2Zr0.1Sc	Balance	4.0	0.7	0.4	0.2	0.1
2	Al4Ca0.7Mn0.4Fe0.4Zr	Balance	4.0	0.7	0.4	0.4	–

Table 2

Annealing regimes

Designation	Regime
T250	250 ^{o}C, 3h
T300	T250 + 300 ^{o}C, 3h
T350	T300 + 350 ^{o}C, 3 h
T400	T350 + 400 ^{o}C, 3 h
T450	T400 + 450 ^{o}C, 3 h
T500	T450 + 500 ^{o}C, 3 h

microscopy (TEM, JEM-2100), scanning electron microscopy (SEM, TESCAN VEGA 3) and by electron microprobe analysis (EMPA, OXFORD AZtec). Polished samples were used for the studies. Mechanical polishing was used, as well as electrolytic polishing, which was carried out at a voltage of 12 V in an electrolyte containing six parts C_2H_5OH, one part $HClO_4$ and one part glycerin. The initial analysis of the microstructure of the samples was carried out using OM and detailed metallographic studies were performed using SEM. The thin foils for TEM were prepared by ion thinning with a PIPS (Precision Ion Polishing System, Gatan) machine and studied at 160 kV.

The Brinell hardness was determined in a INNOVATEST (series NEMESIS 9000) hardness testing machine with a ball diameter of 2.5 mm, a load of 612.9 N and a dwell time of 30 s. The specific electrical conductivity (SEC) was measured by eddy-current testing using a VE-26NP device with high purity Al (99.99%) as an additional standard.

Results and discussion

Initially, assuming that the presence of primary intermetallic crystals is certainly undesirable and to estimate the maximum allowable concentrations of iron and manganese, the boundaries of the liquidus surface of the Al − Ca − Mn − Fe − Si system with different calcium contents were calculated (Fig. 1). As can be seen from Fig. 1, in addition to (Al), primary crystals of the Al_6(Fe, Mn) and Al_6Mn phases can also form in this region. With a decrease in the calcium content, the region of the (Al) primary crystallisation is expanded. At 2% Ca, the alloy with 1% Mn admits at least 0.4% Fe
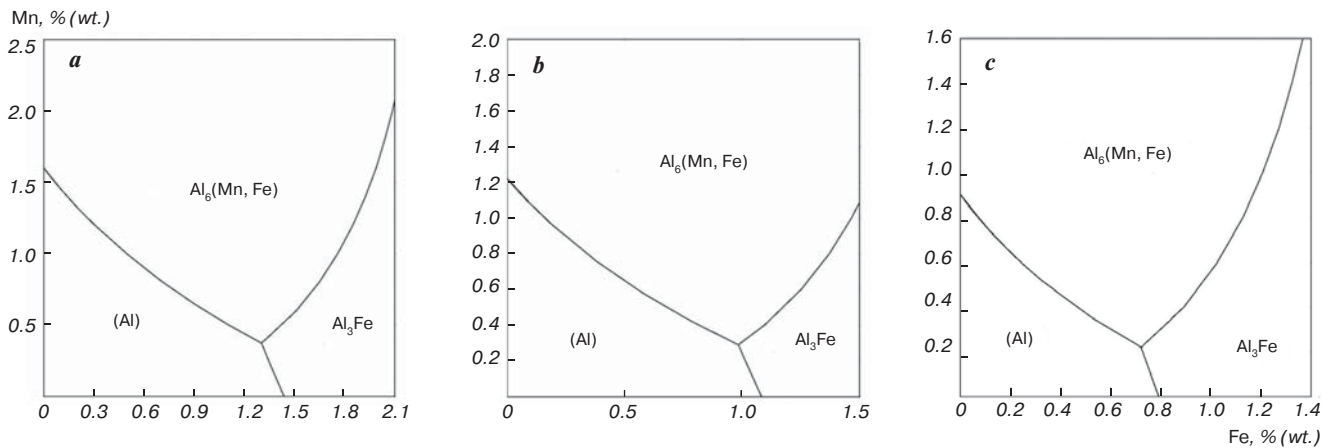

Fig. 1. Liquidus projection of Al − Ca − Mn − Fe − 0.3 Si system at:
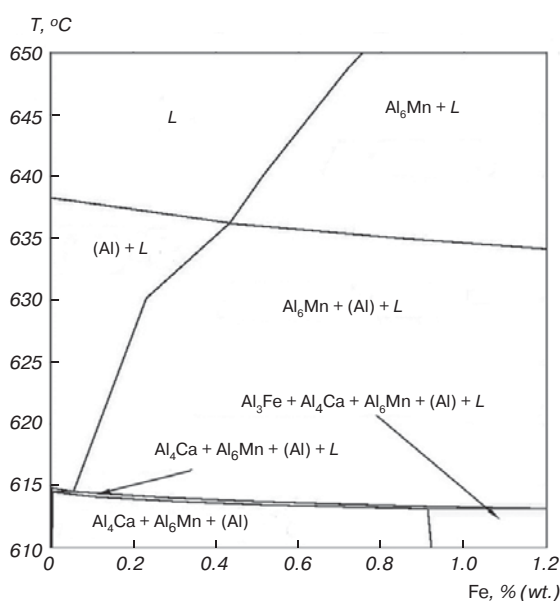a — 2% (wt.) Ca; b —4% (wt.) Ca; c — 6% (wt.) Ca

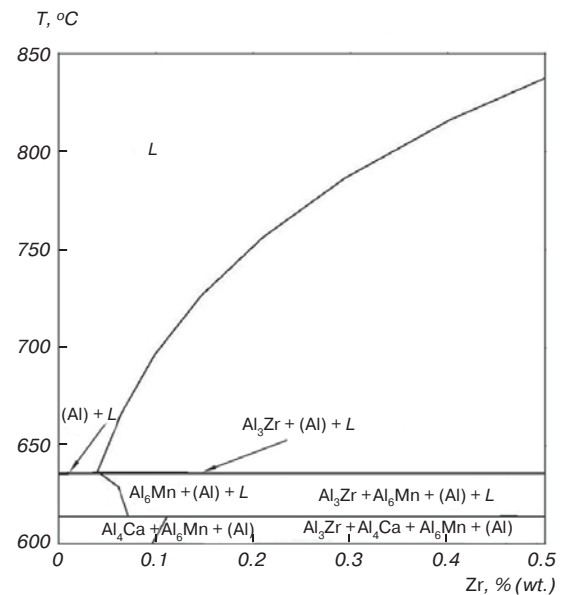**Fig. 2.** Vertical section of Al − Ca − Mn − Fe system at 4% Ca and 0.7% Mn

Fig. 3. Vertical section of Al − Ca − Mn − Fe − Zr − Sc system at 4% Ca, 0.7% Mn, 0.4% Fe and 0.1% Sc

(Fig. 1, *a*), while at 6% Ca, the total concentration of Fe and Mn does not exceed 1% (Fig. 1, *c*). At 4% Ca and 0.7% Mn, the alloy can contain about 0.35–0.40% iron (Fig. 1, *b*). In term to achieving the optimal complex of properties, the last composition Al − 4Ca − 0.7Mn − 0.4Fe seems is the most appropriate.

According to the vertical cross section shown in Fig. 2, during solidification of this alloy, after formation of a the (Al) primary crystals, the eutectic reaction $L \rightarrow$ (Al) + + Al_6(Fe, Mn) should occur. Solidification of this alloy should be completed via the four-phase eutectic reaction $L \rightarrow$ (Al) + Al_6(Fe, Mn) + Al_4Ca, which has a very small temperature range (less than 1 °C, see callout in Fig. 2). Since the total temperature range of solidification of the Al − 4% Ca − 0.7% Mn − 0.4% Fe alloy is relatively small (~20 °C), we would expect good castability.

The influence of zirconium and scandium on the boundaries of the appearance of primary crystals of intermetallic phases in the selected alloy is reflected in Fig. 3, from which we can see that at 0.20% Zr, the Al_3Zr aluminide should initially form. However, it is known that at the cooling rates typical for the casting in metal moulds (5−20 °C/s), the concentration boundary is shifted toward higher zirconium concentrations [10, 11, 16]. Therefore, it was assumed that the total amount of Zr and Sc should enter into the (Al) composition and consequently have no influence on the phase composition of the Al − 4% Ca − 0.7% Mn − 0.4% Fe alloy, as considered above. However, when these additions are present, the casting temperature should be higher than for the base alloy, which is associated with an increase in the liquidus temperature. This follows from the vertical section shown in Fig. 3.

Microstructure and hardening of Al4Ca0.7Mn0.4FeZrSc alloy

In accordance with empirical data, we proceed from the fact that in the as-cast state the entire amount of zirconium and scandium should completely include in the (Al). For experimental studies, we considered two compositions: the first one with 0.1% Sc plus 0.2 % Zr (which seems is most optimal according to [16]) and second one with 0.4 % Zr.

The microstructure of the both alloys, are shown in Fig. 4 and 5, looks reasonably uniform. In accordance with the results of thermodynamic calculations, in the structure of the alloys no primary crystals of intermetallic phases were detected. The main structural components are both primary crystals of (Al) and eutectic colonies with a fine structure. No significant differences in the microstructure of both alloys were also observed. The rounded (Al) dendritic cells, whose average size is ~20– 30 μm are surrounded by a eutectic, the dimensions of individual crystals of intermetallic phases in which less than 1 μm (Fig. 4 and 5, *c*, *d*). Calcium is concentrated in the eutectic (Fig. 6, *b*). On the general background of the

eutectic, separate regions with an increased content of iron (Fig. 6, *c*) are found. This allows us to identify them as the Al_6(Fe, Mn) phase, which formed in the process of the $L \rightarrow$ (Al) + Al_6(Fe, Mn) eutectic reaction (as follows from Fig. 2). In comparison with the rest of the eutectic, these crystals are bright in appearance and have a slightly coarser structure. Scandium, zirconium and manganese, as can be seen from Fig. 6, *d–f*, enter not only in the eutectic composition, but also in the (Al) primary crystals, what gives the reason to expect hardening during subsequent annealing of the alloy.

Quantitative analysis of the chemical composition of (Al) shows that the manganese (Tables 3 and 4) concentration is close to its concentration in the alloy (Table 1). The concentration of scandium in (Al) is also close to its concentration in the alloy. The higher measured zirconium concentration is probably due to the fact that its distribution coefficient is greater than 1 and
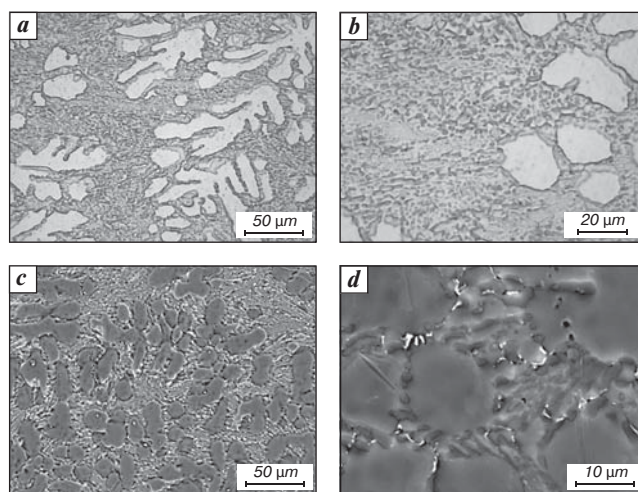

Fig. 4. Microstructure of experimental alloy Al4Ca0.7Mn0.4Fe0.2Zr0.1Sc in as-cast state:
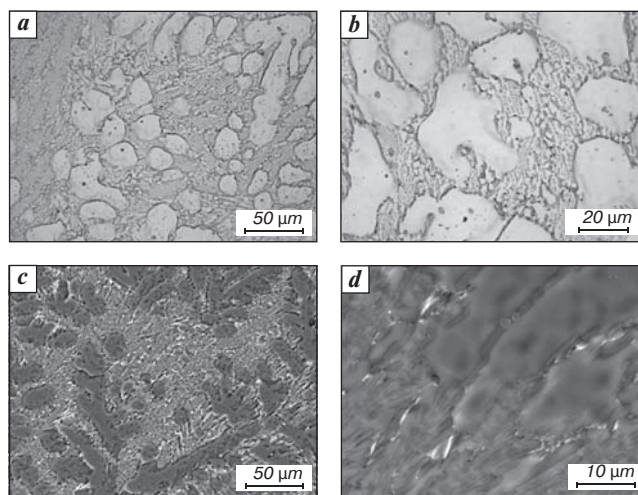*a*, *b* — OM; *c*, *d* — SEM

Fig. 5. Microstructure of experimental alloy Al4Ca0.7Mn0.4Fe0.4Zr in as-cast state:
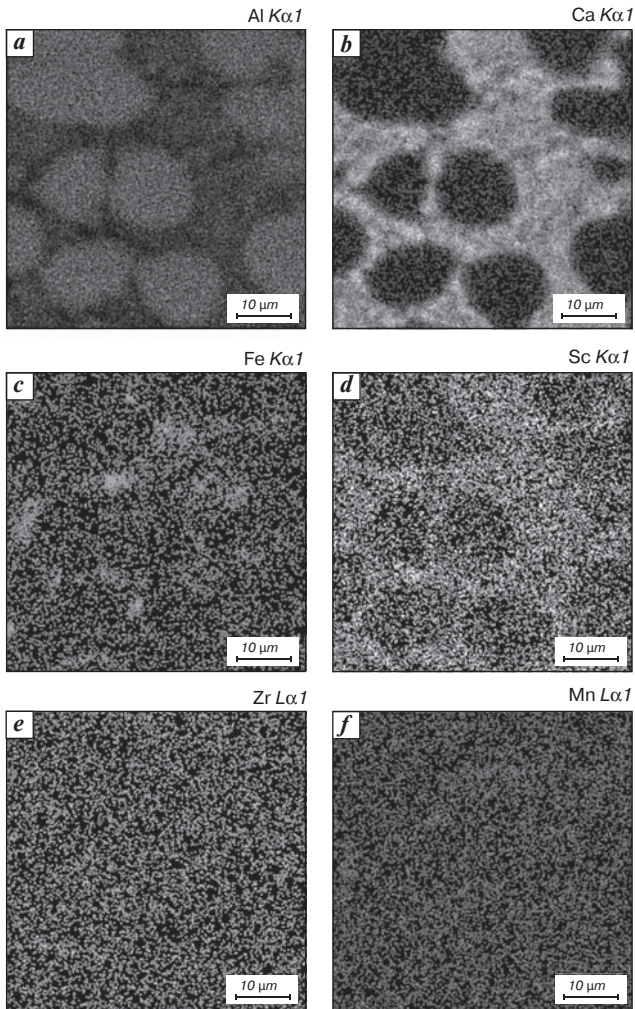*a*, *b* — OM; *c*, *d* — SEM

Fig. 6. EMPA elemental mapping of (*a*) Al, (*b*) Ca, (*c*) Fe, (*d*) Sc, (*e*) Zr and (*f*) Mn for the as-cast alloy Al4Ca0.7Mn0.4Fe0.2Zr0.1Sc

Fig. 7. Effect of annealing temperature on (a) hardness and (b) specific electrical conductivity (SEC) of alloys Al4.5Ca0.7Mn0.3Fe0.2Si-0.4Zr (*1*) and Al4.5Ca0.7Mn0.3Fe0.2Si-0.2Zr-0.1Sc (*2*)

Fig. 8. Precipitates of (*a*) $Al_3(Zr, Sc) - L1_2$ (bright field) and (*b*) Al_6Mn (dark field) in Al4Ca0.7Mn0.4Fe0.2Zr0.1Sc alloy after annealing 250 °C, 3h + 300 °C, 3h. TEM

Table 3

Chemical composition of aluminium solid solution in as-cast alloy Al4Ca0.7Mn0.3Fe0.2Zr0.1Sc

Concentration, % (wt.)					
Ca	Mn	Fe	Zr	Sc	Al
0.01±0.02	0.75±0.09	0.02±0.04	0.49±0.15	0.07±0.02	Balance

Table 4

Chemical composition of aluminium solid solution in as-cast alloy Al4Ca0.7Mn0.3Fe0.4Zr

Concentration, % (wt.) (% (at.))[1]				
Ca	Mn	Fe	Zr	Al
0.03±0.01	0.07±0.15	0.01±0.043	0.55±0.10	Balance

as a result it is predominantly concentrated in the centres of the dendritic cells [17], into which the electron probe was focused. The contents of iron and calcium in (Al), as expected, are negligible.

The presence of a given amount of Zr and Sc in (Al) in the as-cast state suggests the possibility of precipitation hardening du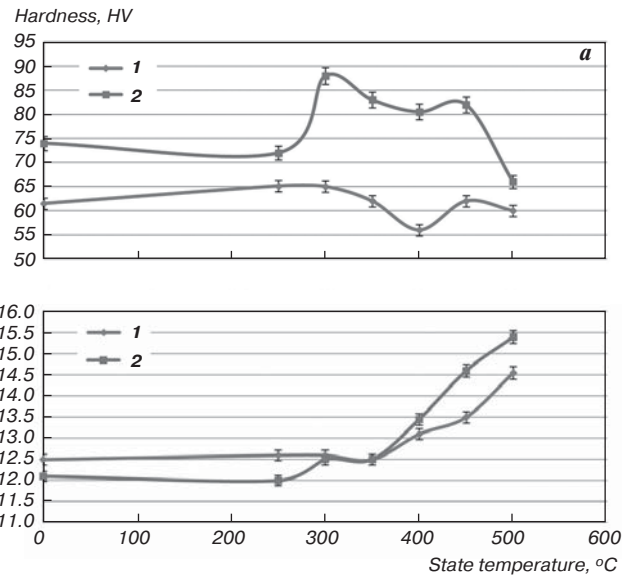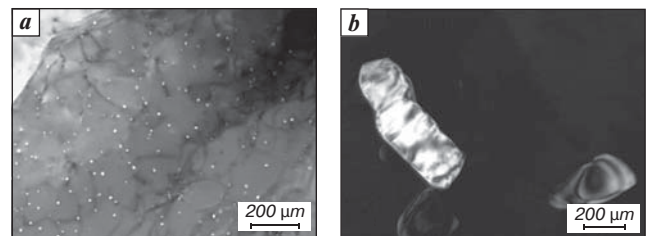e to (Al) decomposition during annealing. This process has been studied using the measurements of hardness and specific electrical conductivity, as well as TEM. As can be seen from Fig. 7, *a*, the alloy with a zirconium content of 0.4% virtually does not hardening during annealing. At 400 °C, the hardness of the alloy reaches a minimum, which can be explained by the complete decomposition of the aluminum solid solution. A further increase in hardness with increasing annealing temperature can be associated with an increase in the solubility of elements in aluminium. The specific electric conductivity curve increases throughout the whole annealing temperature range and at 400 °C has a characteristic inflection directed toward increasing electrical conductivity.

Much more significant results were obtained for the alloy with zirconium and scandium. The peak of hardness, which is ~19% higher than the initial cast state, is reached at 300 °C. A further increase in the annealing temperature leads to a smooth decrease in hardness. At a temperature of 400 °C, a second peak appears, slightly smaller than the first. The appearance of the second peak may be associated with the influence of the zirconium additive. Thus, the combined introduction of 0.1% Sc and 0.25%

Zr provides not only a hardening effect, but also increases the softening temperature (i. e., thermal stability). The specific conductivity curve for this alloy also increases throughout the whole annealing temperature range and at 300 ^{o}C contains an inflection directed toward increasing electrical conductivity. This inflection is associated with the decomposition of (Al).

The TEM structures, shown in Fig. 8, confirm the presence of secondary precipitates containing zirconium and scandium, in the state of maximum hardening of the alloy. In particular, the darkfield images show the presence of uniformly located particles of the $Al_3(Zr, Sc) - L1_2$ phase, with a size of less than 10 nm (Fig. 8, *a*). The presence of secondary precipitates of the Al_6Mn phase with an orthorhombic lattice is reflected in Fig. 8, *b*. The size of these precipitates is ~200 nm, which is quite typical [18].

In general, the experimental alloy structure is reasonably suitable to expect a sufficiently high complex of mechanical and physical properties.

Conclusions

1. By using the thermodynamic calculation in the Thermo-Calc program, an analysis of the $Al - Ca - Mn - Fe - Zr - Sc$ phase diagram, including the construction of the liquidus projection and vertical sections were carried out. Based on the obtained results, the optimal concentrations of calcium (4%) and manganese (0.7%) at an allowable iron content of up to 0.4% for the new alloy were chosen.

2. Experimental analysis of the microstructure of two alloys with different content of zirconium and scandium: Al4Ca0.7Mn0.4Fe0.2Zr0.1Sc and Al4Ca0.7Mn0.4Fe0.4Zr has revealed that in both cases it consists of the (Al) primary crystals and eutectic colonies with a fine structure. Calcium and iron are concentrated in the eutectic, while scandium, zirconium and manganese were detected in the both eutectic composition and (Al) primary crystals.

3. Analysis of the hardness and specific electrical conductivity together with transmission electron microscopy has revealed that joint alloying with zirconium and scandium (0.20% Zr and 0.1% Sc) leads to the precipitation hardening due to the decomposition of (Al) and further precipitation of the coherent $L1_2 - Al_3(Zr, Sc)$ phase nanoparticles.

References

1. Belov N. A., Naumova E. A., Alabin A. N., Matveeva I. A. Effect of scandium on structure and hardening of Al–Ca eutectic alloys. *Journal of Alloys and Compounds*. 2015. Vol. 646. pp. 741–747.

2. Belov N., Naumova E., Akopyan T. Eutectic alloys based on the $Al - Zn - Mg - Ca$ system: microstructure, phase composition and hardening. *Materials Science and Technology*. 2017. Vol. 33. pp. 656–666.

3. Swaminathan K., Padmanabhan K. A. *Journal of Materials Science*. 1990. Vol. 25. pp. 4579–4586.

4. Belov N. A., Naumova E. A., Akopyan T. K., Doroshenko V. V. Phase Diagram of $Al - Ca - Mg - Si$ System and Its Application for the Design of Aluminum Alloys with High Magnesium Content. *Metals*. 2017. Vol. 7(10). p. 429.

5. Kaufman J. G., Rooy E. L. Aluminum alloy castings: properties, processes, and applications, ASM International, Ohio, 2004.

6. Hatch J. E. (Ed.), Aluminum: properties and physical metallurgy, ASM International, Ohio, 1984.

7. Marquis E. A., Seidman D. N. Nanoscale structural evolution of Al3Sc precipitates in Al (Sc) alloys. *Acta Materialia*. 2001. Vol. 49. pp. 1909–1919.

8. Costa S., Puga H., Barbosa J., Pinto A. M. P. The effect of Sc additions on the microstructure and age hardening behaviour of as cast Al–Sc alloys. *Materials and Design*. 2012. Vol. 42. pp. 347–352.

9. Knipling K. E., Karnesky R. A., Lee C. P., Dunand D. C., Seidman D. N. Precipitation evolution in Al–0.1Sc, Al–0.1Zr and Al–0.1Sc–0.1Zr (at.%) alloys during isochronal ageing. *Acta Materialia*. 2010. Vol. 58. pp. 5184–5195.

10. Clouet E., Barbu A., Lae L., Martin G. Precipitation kinetics of Al_3Zr and Al_3Sc in aluminum alloys modeled with cluster dynamics. *Acta Materialia*. 2005. Vol. 53. pp. 2313–2325.

11. Lefebvre W., Danoix F., Hallem H., Forbord B., Bostel A., Marthinsen K. Precipitation kinetic of Al3(Sc,Zr) dispersoids in aluminium. *Journal of Alloys and Compounds*. 2009. Vol. 470. pp. 107–110.

12. Zhou W. W., Cai B., Li W. J., Liu Z. X., Yang S. Heat-resistant Al–0.2Sc–0.04Zr electrical conductor. *Materials Science and Engineering A*. 2012. Vol. 552. pp. 353–358.

13. Booth-Morrison C., Mao Z., Diaz M., Dunand D. C., Wolverton C., Seidman D. N. Role of silicon in accelerating the nucleation of $Al_3(Sc,Zr)$ precipitates in dilute $Al - Sc - Zr$ alloys. *Acta Materialia*. 2012. Vol. 60. pp. 4740–4752

14. Tian L., Kim H., Anderson I., Russell A. The microstructure-strength relationship in a deformation processed Al–Ca composite. *Materials Science and Engineering A*. 2013. Vol. 570. pp. 106–113

15. Kendig K., Miracle D. Strengthening mechanisms of an $Al - Mg - Sc - Zr$ alloy. *Acta Materialia*. 2002. Vol. 50. pp. 4165–4175.

16. Booth-Morrison C., Mao Z., Diaz M., Dunand D. C., Wolverton C., Seidman D. N. Role of silicon in accelerating the nucleation of $Al_3(Sc,Zr)$ precipitates in dilute Al–Sc–Zr alloys. *Acta Materialia*. 2012. Vol. 60. pp. 4740–4752

17. Kaufman J. G., Rooy E. L. Aluminum alloy castings: properties, processes, and applications, ASM International, Ohio, 2004.

18. Vlach M., Stulikova I., Smola B., Piesova J., Cisarova H., Danis S., Plasek J., Gemma R., Tanprayoon D., Neuber V. Effect of cold rolling on precipitation processes in $Al - Mn - Sc - Zr$ alloy. *Materials Science and Engineering A*. 2012. Vol. 548. pp. 27–32.

NFM